Research Article

Preparation and Evaluation of Smart Nanocarrier Systems for Drug Delivery Using Magnetic Nanoparticle and Avidin-Iminobiotin System

Shuguo Sun,[1,2] **Beiping Li**,[1] **Tao Yang**,[1] **Meihu Ma**,[2] **Qinlu Lin**,[1] **Juanhong Zhao**,[1] **and Feijun Luo**[1,3]

[1]*National Engineering Laboratory for Rice and Byproduct Processing, Central South University of Forestry and Technology, Changsha, Hunan 410004, China*
[2]*National R&D Center for Egg Processing, Huazhong Agricultural University, Wuhan, Hubei 430070, China*
[3]*Department of Pathology, Addenbrooke's Hospital, University of Cambridge, Cambridge, UK*

Correspondence should be addressed to Tao Yang; yangtao807@163.com and Meihu Ma; mameihuhn@163.com

Received 30 March 2018; Accepted 27 May 2018; Published 28 August 2018

Academic Editor: Vidyadhar Singh

Therapeutic efficacy and the regulation of drug release can be improved by using selective targeting drug delivery systems. In this paper, we have demonstrated avidin-immobilized magnetic nanoparticles (AMNPs) as a novel targeted drug delivery system to deliver iminobiotinylated daunomycin (IDAU). TEM, XRD, VSM, and FTIR were employed for the physicochemical characterization of the drug-loaded MNPs. The binding of IDAU had little effect on sizes of AMNPs (~35 nm), but the stability and dispersibility of the nanoparticles were improved. The study also found that the loading capacity and efficiency of nanoparticles were mainly dependent on affinity interaction between IDAU and AMNPs. The optimal loading capacity and efficiency of MNPs for IDAU were 0.408 ± 0.012 mg/g and $94.18 \pm 2.64\%$ according to the reversed-phase high-performance liquid chromatography (RP-HPLC) data, respectively. Under the conditions of pH 6.8 and 1 mmol/L of biotin, the drug-loaded MNPs released rapidly at beginning and then maintained at a certain controllable release level. The effect of IDAU on DLKP proliferation was tested, and the results showed that IC50 was $(1.60 \pm 0.05) \times 10^{-3}$ mg/mL. Our findings indicated that AMNPs hold tremendous potential as an effective drug delivery system.

1. Introduction

Preventing the spread of malignant cells in the human body is a matter of serious concern. Presently, surgical resection, radiation, and chemotherapy are generally used to treat the cancer cells, but the selection of the treatment option depends on the location of the tumor and whether the tumor is at an early or advanced stage. Meanwhile, new types of anticancer drugs are being developed unceasingly [1–3], and some drug delivery devices/systems have received considerable attention, such as macromolecular carrier system [4], microcapsule drug delivery system [5], and magnetic drug delivery system [6–8].

The biggest challenge in drug delivery is the transportation of drug agents to the targeted site at the appropriate time [9]. The release rate of conventional administered antitumor drugs or injections is uncontrolled, which may lead to harmful side effects and toxicity due to quick drug release. For an excellent drug delivery system, it must be controllable and then the therapeutic levels can extend over long periods of time, which can eliminate the abovementioned side effects and toxicity. In the controlled delivery, the drug delivery may commence with first-order kinetics to an optimum and effective drug concentration to the targeted site, followed by zero-order kinetics, which may be one of the best ways to release the drug. There are two controlled-release mechanisms for selected drug delivery systems. One mechanism is physical adsorption, and the drug may be automatically released at the appropriate time. Biodegradable polymers, for example, adsorb the drugs due to hydrogen bond and/

or dipole-charge interactions with the polymer chains. The main disadvantage of this system is that it cannot effectively control the rate of drug release. The other mechanism is that the drugs are attached to a carrier through a covalent bond or via an affinity interaction, the most common affinity tag of this type being the avidin-biotin system [10, 11]. This drug delivery system has an advantage that it is influenced by the ambient factors tinily. However, the drugs are difficult to release from the carrier in the condition of pH 6.8. The iminobiotin coupled with anticancer drugs shows a high affinity to avidin (and avidin-immobilized magnetic nanoparticles (AMNPs)) at elevated pH (9.5–10.8) but releases the drugs easily at lower pH (~4) or under the presence of a certain concentration of biotin at pH 6.8 according to the manufacturer's instructions. In this system, the drug release can be controlled under mild conditions. Therefore, the application of avidin-iminobiotin technology in drug delivery systems creates an opportunity for the development of new smart drug delivery systems because of its controllable, easy release of the drug under the condition of pH 6.8.

There is currently a great concern about magnetic field-induced, targeted drug delivery [12–15], in spite of extensive applications of MNPs in biomedical and diagnostic fields and nanoreactor systems, including in vitro cell separation, in vivo antimycotic agent, contrast agent for magnetic resonance imaging, magnetic particle imaging, hyperthermia, tumor therapy, or cardiovascular disease [16–24]. The conjugation of a drug to magnetic nanoparticle (MNP) entrapped polymer or antibody is an effective method for controlled delivery of the drug to the targeted site. Under such medication, the drug can be released at the desired location and act locally until the therapy is completed. Therefore, the dosage of medication can be reduced, and the harmful side effects and toxicity of drugs kept to a minimum [25, 26]. It is worth noting that the MNPs used for the drug delivery system always require adequate magnetic strength, biocompatibility, and functional active groups on the surface [27]. Nanoparticles used in the drug-loaded system will generally be administered by intravenous injection and then transported in the blood. Therefore, the dispersibility and biocompatibility in blood and interaction between plasma proteins and MNPs should be fully considered [28, 29].

The conjugation of a drug to MNPs functionalized with polymer or bioactive macromolecules is a viable method for controlled delivery of a drug to the desired site. In the present study, an iminobiotinylated drug, iminobiotinylated daunomycin (IDAU), was connected to avidin-immobilized magnetic nanoparticles (AMNPs) based on the avidin-iminobiotin binding system. The drug loading capacity and release behavior were then determined through adsorption/dissociation kinetics experiments, and the inhibitory effects of IDAU on liver tumor cell DLKP growth was also evaluated.

2. Experiment

2.1. Materials. Unless stated, all chemicals were commercially available and of analytical grade. EZ-Link® NHS-iminobiotin and DLKP cell medium were purchased from Invitrogen (Life Technologies, Carlsbad, CA, USA). DAU hydrochloride standard preparation was purchased from Sigma. Fetal bovine serum (FBS) was purchased from Hangzhou Sijiqing Company (Hangzhou, China). Other chemicals were of laboratory grade purity and used as obtained.

2.2. Preparation of Functionalized MNPs

2.2.1. Preparation and Glutaraldehyde Activation of PEI-Coated MNPs. MNPs were prepared via a facile solvothermal synthesis method, in which polyethyleneimine (PEI) was used as the protective agent to prevent the particles from aggregation [30]. The typical synthetic procedure was as follows. $FeCl_3{\cdot}6H_2O$ (0.135 g), PEI (0.5 g), and sodium acetate (1.8 g) were added to ethylene glycol (20.0 mL) to form colloid mixture under vigorous stirring at room temperature for 45 min. Then, 18.0 mL of the mixture was sealed in Teflon-lined stainless steel autoclave of 20 mL capacity. Finally, the autoclave was heated and maintained at 200°C for 12 h and allowed to cool down to room temperature naturally. The back products were washed twice with absolute ethanol and twice with Milli-Q water. MNPs were then dispersed in Milli-Q water and stored in sealed cell (50 mL) at room temperature.

To activate PEI-coated MNPs with glutaraldehyde, the nanoparticles were dispersed in 20 mL PBS buffer (0.1 mol/L, pH 8.0) containing 2% glutaraldehyde. The suspension was mechanically stirred at room temperature in the dark for 4 h. The glutaraldehyde-activated MNPs were separated from unconjugated glutaraldehyde by magnetically driven separation at room temperature for 5 min and then washed three times with PBS buffer (0.1 mol/L, pH 8.0). The final glutaraldehyde-activated MNPs were dispersed in 20 mL PBS buffer (0.1 mol/L, pH 8.0) and kept in the dark at 4°C until use.

2.2.2. Immobilization of Avidin onto MNPs. To immobilize avidin, 15 mg of glutaraldehyde activated MNPs was dispersed in 20 mL PBS buffer (0.1 mol/L, pH 8.0) and sonicated for 5 s at 20 W by a Ti probe (Branson 450 sonifier). 5 mL of avidin (100 μg/mL) was introduced to the PBS buffer solution, and the suspension was mechanically stirred at 4°C in the dark for 4 h. AMNPs were separated from unconjugated avidin by magnetically driven separation at 4°C for 5 min and then washed three times with PBS buffer (0.1 mol/L, pH 8.0). The final AMNPs were dispersed in 20 mL PBS buffer (0.1 mol/L, pH 8.0) and kept in the dark at 4°C until use.

2.3. Conjugation of Drug to AMNPs

2.3.1. Preparation of IDAU. IDAU was prepared by reaction between 1.5 mg DAU and 1.0 mg NHS-iminobiotin at 4°C for 24 h in 20 mL of PBS buffer (0.1 mol/L, pH 10.8), and then the buffer was adjusted to pH 8.0 with 1 mol/L phosphoric acid. The product need not be separated from the excessive DAU and kept in the dark at 4°C until use.

2.3.2. Conjugation of IDAU to MNPs. AMNPs were dispersed in 20 mL of PBS buffer (0.1 mol/L, pH 8.0) containing 0.1 mg/mL of IDAU, followed by incubation for 4 h at 4°C with gentle stirring. The DAU-loaded MNPs were separated

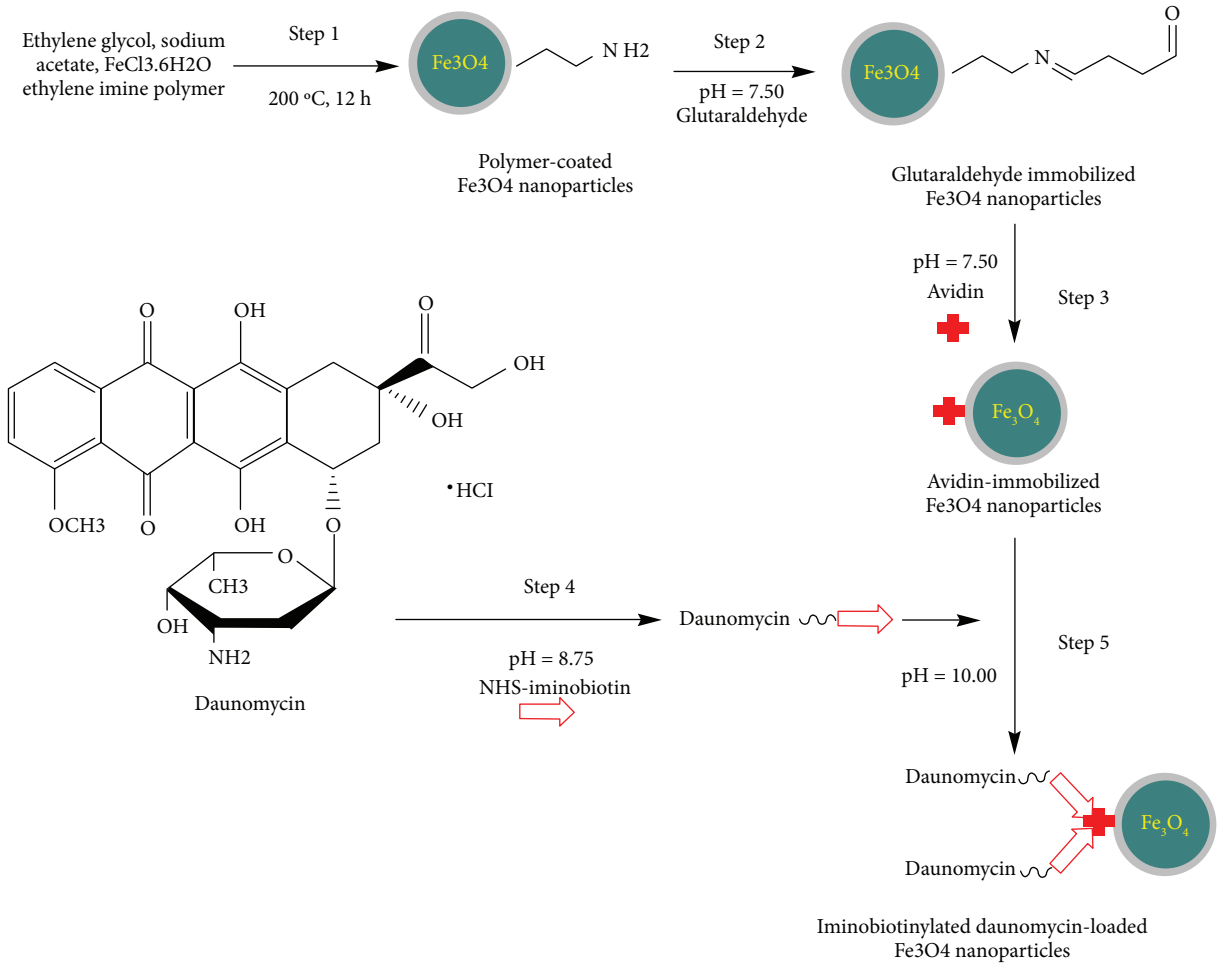

Figure 1: Schematic of the different steps in the preparation of iminobiotinylated daunomycin-loaded Fe_3O_4 nanoparticles.

from the solution with the aid of a magnet and then washed three times with PBS buffer (0.1 mol/L, pH 8.0). The final IDAU-loaded MNPs (IDAU-MNPs) were dispersed in 20 mL PBS buffer (0.1 mol/L, pH 7.0) and kept in the dark at 4°C until use. A schematic of the different steps in the preparation of iminobiotinylated daunomycin-loaded Fe_3O_4 nanoparticles (IDAU-MNPs) is summarized in Figure 1.

2.4. Physicochemical Characterization of MNPs

2.4.1. Particle Shape Analysis and Size Analysis. The size and morphology of AMNPs and DAU-immobilized MNPs were examined under a transmission electron microscope (TEM) operated at 100 KV (model JEM 2010, JeM Inc., Japan). The nanoparticles were first diluted in deionized water to an appropriate concentration (7.5 μg/mL) and then ultrasonicated for 10 s. A copper grid (200 mesh and cover with formvar/carbon) was coated with the thin layer of diluted particle suspension and allowed to stand for 2 min. The excess liquid was drained off by filter paper and the samples were then examined by TEM.

2.4.2. X-Ray Diffraction (XRD). XRD experiments of the crystalline phase of a powder sample of MNPs, AMNPs, and IDAU-MNPs were performed using an X-ray diffractometer (Rigaku D/max-γ, Japan) and Cu-Kα ($\lambda = 0.154056$ nm) radiation. The parameters of the measurements were: 40 kV and 20 mA, angular variation ranging from 20 to 80° in steps of 10.0° for each 1 min (geometry θ–2θ).

2.4.3. Vibrating-Sample Magnetometry (VSM). MNPs, AMNPs, and IDAU-MNPs were checked for magnetic susceptibility using vibrating-sample magnetometer (PARC, 155, USA) which provided magnetization (emu g^{-1}) of magnetic particles in response to an external magnetic field (Oe).

2.4.4. Fourier-Transform Infrared Spectroscopy (FTIR). Avidin and DAU anchoring onto the surface of MNPs were monitored by FTIR. Data were collected on a Nicolet Avatar-330 Spectrometer (Thermo Nicolet, USA) with 4 cm^{-1} resolution using the KBr pellet technique.

2.5. Drug Loading Determination (Indirect Estimation). The degree of IDAU incorporation into AMNPs was analyzed by RP-HPLC and monitored using a UV-VIS detector. IDAU-MNPs were separated from unconjugated DAU and IDAU by magnetically driven separation at 4°C for 5 min and then rinsed with PBS buffer (0.1 mol/L, pH 8.0) until

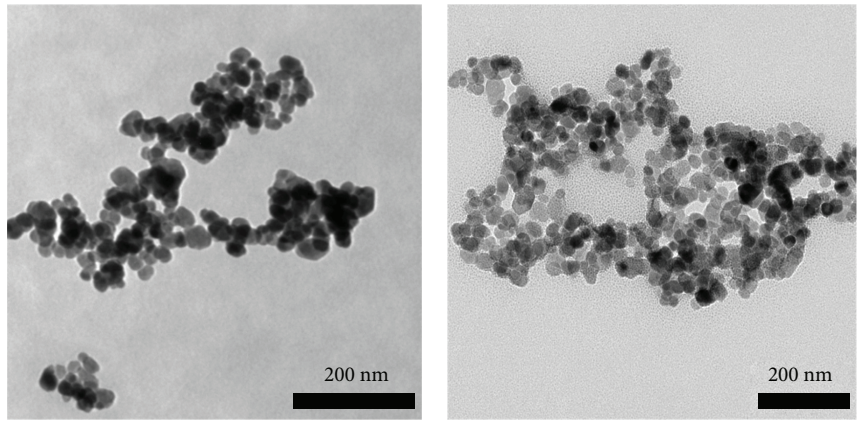

(a) (b)

Figure 2: TEM images of AMNPs (a) and IDAU-MNPs (b).

no DAU was detected in washings. The IDAU loading capacity (LC, mg/g) was determined as

$$\mathrm{LC(mg/g)} = 100 \times \frac{C_{\mathrm{d}}}{C_{\mathrm{n}}} = 100 \times \frac{(C_0 - C_1)}{C_{\mathrm{n}}}, \quad (1)$$

where C_{d}, C_{n}, C_0, and C_1 are the concentrations of IDAU incorporated in nanoparticles (mg/mL), MNPs offered for DAU incorporation (g/mL), initial additions of IDAU (mg/mL), and IDAU remained in PBS buffer after the DAU-loaded MNPs were separated from the solution (mg/mL), respectively.

2.6. In Vitro Evaluation of the Anticancer Drug

2.6.1. Kinetics of Drug Release. Two methods for drug release were investigated in our experiments. On the one hand, appropriate amounts of IDAU-MNPs samples were dispersed in 20 mL of incubation medium (PBS buffer containing 1 mM of biotin, pH 6.8) and maintained under constant mild agitation in a water bath (37°C). On the other hand, the same amounts of drug-loaded MNPs samples were dispersed in 20 mL of 0.1 mol/L ammonium acetate buffer at pH 4.0 (the buffer containing 0.5 mol/L NaCl and 1.0 mmol/L EDTA) and maintained under constant mild agitation in a water bath (37°C). The final concentration of IDAU was chosen to ensure sink conditions for the in vitro study. Aliquots (15 μL) were taken in predetermined time intervals from 2 to 540 min. Each aliquot was analyzed with RP-HPLC for IDAU content as described above.

2.6.2. In Vitro Cytotoxicity. A proliferation method was used to measure the cytotoxicity of IDAU-MNP samples towards the DLKP cell line [30–33], with slight modifications. Cytotoxicity of drugs was measured as previously described. Briefly, cells were seeded at 1×10^3 cells/well in a 96-well plate and left to attach overnight in a 5% CO_2 incubator at 37°C. The appropriate concentrations of IDAU-MNPs were prepared freshly at twice their final concentration and added to the plate on the following day. The assay was terminated after further 7-day incubation. The effect of treatment was examined by comparing the growth of cells in the treated rows to the growth of cells in the control rows and expressed as percentage. All assays were performed at least in triplicate.

3. Results and Discussion

3.1. Physicochemical Characterization of MNPs

3.1.1. Transmission Electron Microscope and X-Ray Diffraction. Typical TEM micrographs for AMNPs and IDAU-MNPs were shown in Figures 2(a) and 2(b), respectively, which indicated that the diameter of these particles was approximately 35 nm. The shape of MNPs was spherical and its particles were well-distributed. After the IDAU was connected to AMNPs, no significant difference in sizes of AMNPs and IDAU-MNPs were observed, but the IDAU-MNPs had more uniform size distribution. Because of these features of MNPs described above, MNPs had good stability, better dispersibility, huge surface area, and greater loadspace. It was also observed in our study that the dispersity and stability of MNP-loaded IDAU increased compared to AMNPs, indicating that the hydrophilic groups on the MNP surface increased and the biocompatibility of MNPs enhanced when IDAU was loaded onto the nanoparticles.

Crystallinity and crystal size are important properties to be considered for the present study as they affect the magnetic susceptibility. X-ray diffraction is a useful technique for characterizing the crystalline samples. XRD patterns (Figure 3(a)) of MNPs, AMNPs, and IDAU-MNPs were used for determining the crystallographic identity and phase purity and for calculating the average crystallite diameter based on the full width at half maximum (FWHM) in the XRD profile. There were 6 peaks at 30.14, 35.47, 43.14, 53.45, 57.08, and 62.63 (2θ) in the XRD profile, which was characteristic of Fe_3O_4. It was confirmed by ICDD database (reference code 01076-0955) and showed 100% purity. The average crystallite size of MNPs was calculated by the X-ray line broadening method by the use of Debye–Scherrer's equation taking FWHM of peak at 35.47 (2θ) as this peak showed least interferences, giving the average particle size of about 30.02, 35.46, and 35.61 nm for MNPs, AMNPs,

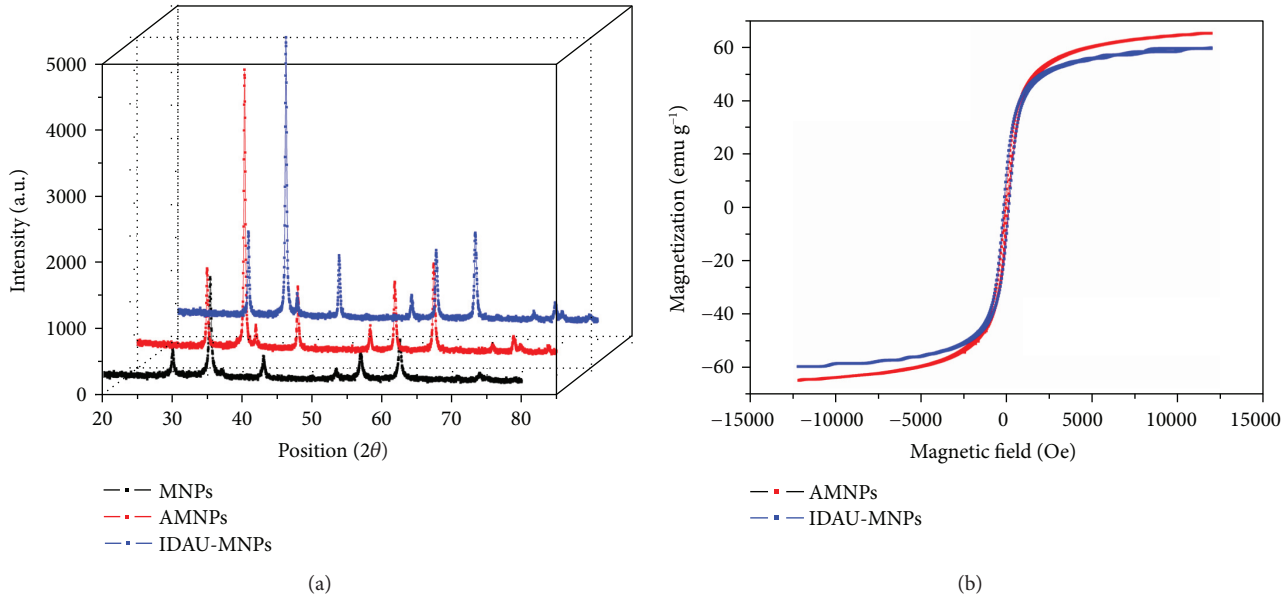

Figure 3: XRD diffractogram of MNPs (black), AMNPs (red), and IDAU-MNPs (blue) (a) and the magnetic hysteresis loops for AMNPs (red) and IDAU-MNPs (blue) (b).

and IDAU-MNPs, respectively. These sizes are in agreement with the sizes measured by TEM.

It is very important that the prepared MNPs possesses sufficient magnetic and superparamagnetism property for practical application. Figure 3(b) displayed the VSM magnetization curves of AMNPs and IDAU-MNPs at room temperature; the results indicated the saturation magnetization of AMNPs and IDAU-MNPs were 64.92 and 59.63 emu g^{-1}, respectively. All of the magnetic nanoparticles showed quasi-superparamagnetic behavior and had little remanence and coercivity. Drug loading into MNPs in significant amounts resulted in the slight decrease in magnetic strength of the composite because of the weight contribution from the nonmagnetic portion. The saturation magnetization of IDAU-MNPs was sufficient for the magnetically driven transport of drugs with a conventional magnet.

3.1.2. Fourier-Transform Infrared Spectroscopy (FTIR). FTIR spectroscopy is an appropriate technique to confirm drug insertion into the nanoparticles. In the FTIR spectrum of AMNPs (Figure 4(a)), three strong bands were observed at 568.0, 1637.1, and 1655.4 cm^{-1}. The first was due to the Fe-O stretching mode of the Fe_3O_4 MNPs, and the second and third were associated with the α-helical and β-folded types of secondary structure of avidin, respectively [34, 35]. The presence of two bands at 1637.1 and 1655.4 cm^{-1} confirmed that avidin was immobilized successfully on Fe_3O_4 MNPs.

In the FTIR spectrum of IDAU (Figure 4(b)), the characteristic C=O (hydrogen-bonded quinone carbonyl group), C=C, and C-OH stretching modes of IDAU were observed at 1618.0, 1578.1, and 1115.9 cm^{-1}, respectively [36], and there was a large difference in intensity between the two strong bands at 1618.0 and 1578.1 cm^{-1}. However, in the FTIR spectrum of DAU, two strong bands of similar intensity were found at 1617.0 and 1580.0 cm^{-1} [37]. The

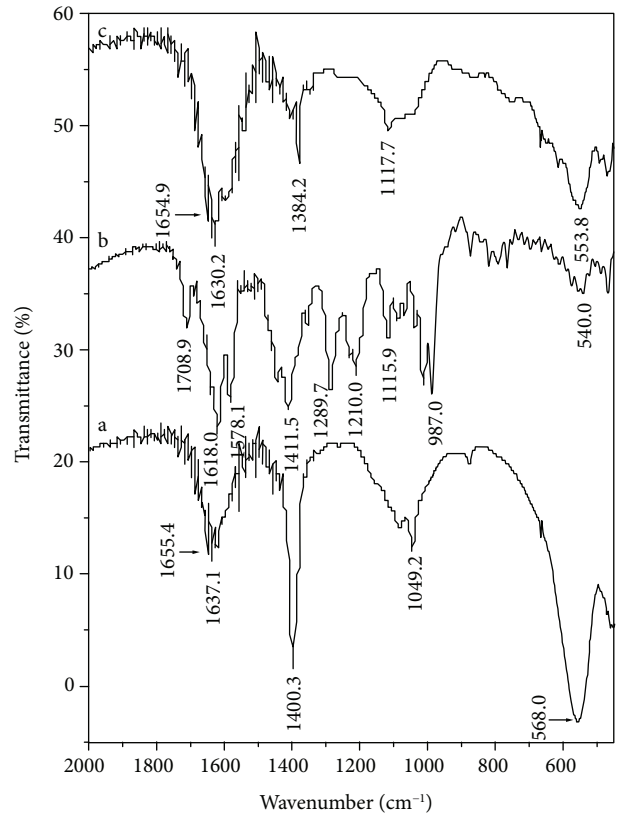

Figure 4: FTIR spectra of avidin-immobilized magnetic nanoparticles (a), daunomycin (b), and iminobiotinylated daunomycin-loaded magnetic nanoparticles (c).

intensity changes in the infrared spectra showed that the molecular structure of DAU was changed after it was 2-iminobiotinylated. Furthermore, the characteristic C-O and

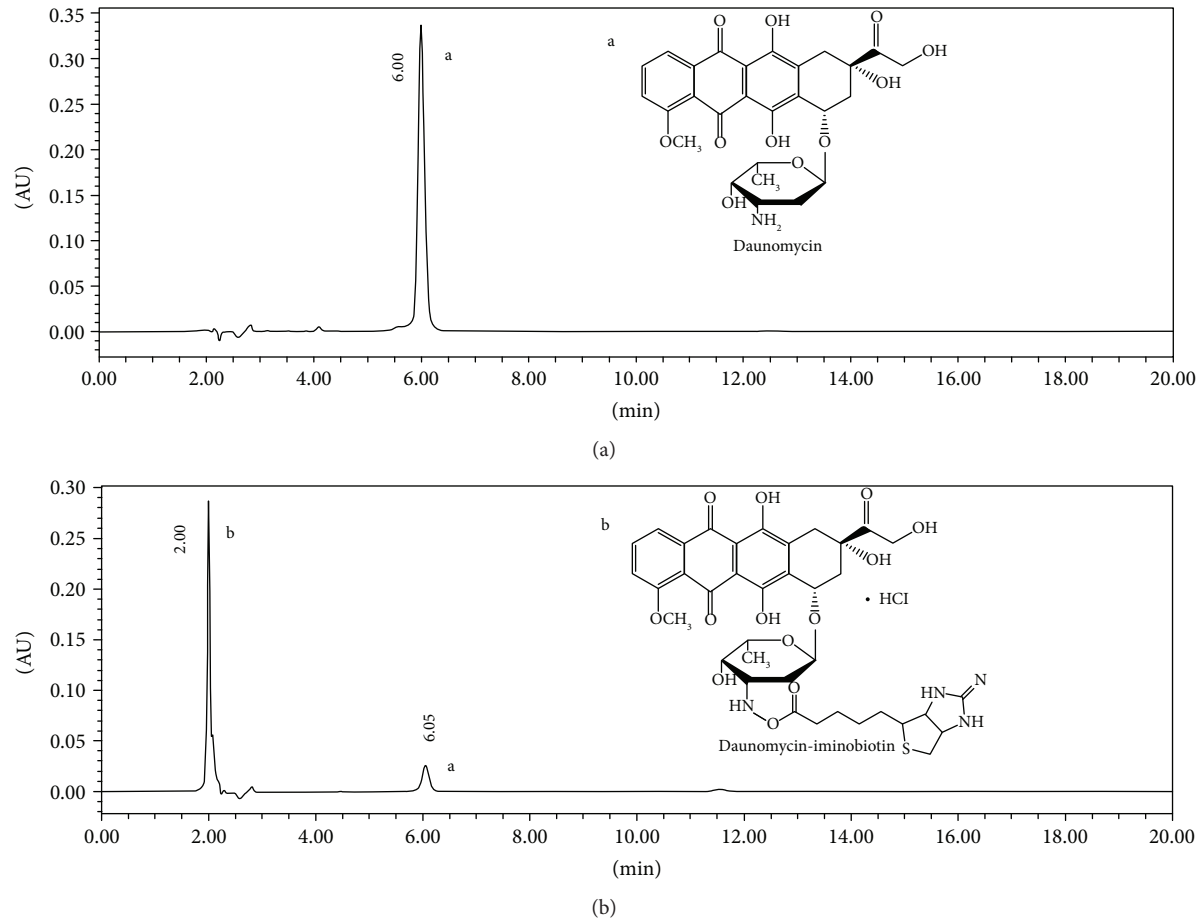

Figure 5: HPLC analysis of the mixtures containing only daunomycin (a), iminobiotinylated daunomycin, and daunomycin (b).

N-H stretching modes of IDAU were also observed at 1210.0 and 1289.7 cm^{-1}, respectively [38], but they were not found in DAU, which indicated IDAU was successfully prepared by reaction between DAU and NHS-iminobiotin.

In the FTIR spectrum of IDAU-MNPs (Figure 4(c)), the characteristic absorption of Fe-O bond of drug-loaded MNPs was discovered at 553.8 cm^{-1}, which shifted from 568.0 to 553.8 cm^{-1} (Figure 4(a)). The characteristic C-OH stretching mode of drug-loaded MNPs was observed at 1117.7 cm^{-1}. There was strong evidence for the presence of drug molecules in MNPs. However, the characteristic bands (such as at 1618.0 and 1578.1 cm^{-1}) of IDAU could not be found after it was connected to MNPs, with the exception of the band assigned to C-OH, which shifted from 1115.9 to 1117.7 cm^{-1} (Figure 4(b)). The absence of the two characteristic bands confirmed a strong interaction between IDAU and AMNPs.

3.2. Drug Loading Determination

3.2.1. Determination of DAU and IDAU. RP-HPLC adopted to determine DAU has the advantages of high sensitivity and good reproducibility. The chromatogram of RP-HPLC determining DAU was shown in Figure 5(a). According to the result, the retention time of DAU was at 6.00 min, and the intralaboratory reproducibility was very good, with 90% of the replicates analyzed in the same laboratory differing by ≤2.8%. The regression equation for determining DAU was established through several experiments ($y = 31139161.20x - 54373.54$, where y was the peak area and x was the concentration of DAU, $R^2 = 0.9995$). IDAU was generated by reaction of DAU with NHS-iminobiotin in alkaline condition. The best rate of DAU acylation determined by the above formula was 78.90 ± 2.13%. After the reaction between excessive DAU and NHS-iminobiotin, RP-HPLC was used to analyze IDAU. The chromatogram of the DAU and IDAU mixture was shown in Figure 5(b). The results showed that the separation effect of liquid chromatography about these two substances was very good, and the retention time of DAU excessed was at 6.05 min, while the retention time of IDAU was at 2.00 min. Here, we created a standard curve and used linear regression analysis (called a trendline in excel) to determine the concentration of IDAU ($y = 31139161.20x - 54373.54$, where y was the peak area and x was the concentration of IDAU, $R^2 = 0.9991$).

3.2.2. Adsorption Dynamics of IDAU on AMNPs. The drug loading efficiency of MNPs and their loading capacity are two important indicators for the drug delivery system. For this reason, the IDAU loading efficiency of MNPs and their

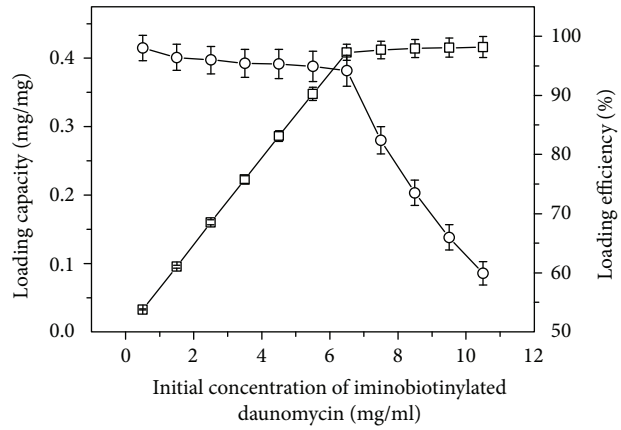

Figure 6: Dependence of the loading capacity (□) and loading efficiency (○) on initial concentration of iminobiotinylated daunomycin used during the preparation. Each result is the average calculated in 95% confidence interval of five parallel studies.

loading capacity were studied using indirect RP-HPLC analysis. The results were presented in Figure 6. When the initial concentration of IDAU was less than 7 mg/mL, the loading efficiency of more than 90% was observed. However, upon increasing the initial drug concentration, the loading efficiency decreased rapidly, but the drug adsorption capacity was unchanged. This strongly suggested that the drug adsorption behaviors were mainly dependent on affinity interaction between IDAU and AMNPs, and the nonspecific adsorption of the drug was extremely low. The same phenomenon could also be observed in the other molecular adsorption processes using the avidin-biotin binding system [39–41]. The increase of the initial concentration of IDAU needs more iminobiotin binding sites of AMNPs. When the iminobiotin binding sites of AMNPs were not sufficiently high (saturation) with increasing IDAU concentration, the amount of specific adsorption capability for IDAU was unchanged. Therefore, the optimum initial concentration of IDAU was 7 mg/mL, and the loading capacity and loading efficiency of MNPs were 0.408 ± 0.012 mg/g and $94.18 \pm 2.64\%$, respectively. Compared with the drug loaded into MNPs through physical encapsulation or adsorption, the drug connected to AMNPs based on the avidin-iminobiotin system would not be easily released during transportation of the drug due to the effects of environmental parameters such as temperature, pH, ionic strength, and sodium nitrate. The drugs could be delivered to the targeted site at the appropriate time successfully. The controllable drug delivery system could maximize its bioefficacy, reduce the side effects, and facilitate clinical applicability [42].

3.3. Performance Evaluation of Drug-Nanoparticle Formulations

3.3.1. In Vitro Drug Release. The in vitro drug release from IDAU-MNPs was monitored as a function of time in PBS buffer at pH 6.8 or in ammonium acetate buffer at pH 4.0 as shown in Figures 7(a) and 7(b), respectively. For method 1, IDAU could be completely released from MNPs for 30 min at pH 4.0, but the drug did not readily dissociate at pH 6.8. The reason was that the drug release behavior from nanoparticles was mainly dependent on the interaction between IDAU and AMNPs at different pH values [43–45]. Practical applications of method 1 in the clinical laboratory were limited because of the rapid and transient release of the drug and its strict dissociation conditions. For method 2, IDAU was released by adding a certain concentration of biotin at pH 6.8, because under that specific condition, the strength of affinity interaction between biotin and AMNPs was more than that of iminobiotin and AMNPs, and IDAU was replaced by biotin. Fortunately, the conditions were relatively mild. The amount of IDAU released to the outer medium was measured using RP-HPLC, and the drug release data were presented in Figure 7(c). A low concentration of biotin (1 mmol/L) was used in our research. The results showed that the initial stage was characterized by a fast release of a limited quantity of IDAU, and the second stage was described by a slow, steady, and controlled release of the drug. The maximum concentration of IDAU released to the outer medium was strongly correlated with the concentration of IDAU loading on MNPs, but the maximum concentration of IDAU loading on MNPs did not release the maximum concentration of IDAU at the same concentration of biotin. The release profiles exhibited strong dependence on the concentration of IDAU connected to MNPs. When the concentration was 0.015 mg/mL, 38.9% of the loaded drug could be released within 150 min, and the concentration of the drug released was 5.84 μg/mL. When the concentration of IDAU connected to MNPs was 0.055 mg/mL, only 10.5% of the loaded drug could be released within the same time, and the concentration of the drug released was 5.78 μg/mL. However, when the concentration of the drug connected to MNPs was 0.035 mg/mL, the concentration of the drug released could reach 6.49 μg/mL. According to these results, it could be concluded that the optimum concentration of IDAU connected to MNPs was 0.035 mg/mL. The different concentrations of the drug released might be attributed to the interaction between biotin and drug-loaded MNPs, and the interaction was a complex, dynamic process. The first process was the dissociation of IDAU from AMNPs at pH 6.8. At the same time, a high concentration of biotin and strong affinity interaction between biotin and avidin at pH 6.8 promoted the interaction between biotin and AMNPs, and the loaded IDAU would be rapidly released. When the dissociation reactions between IDAU and AMNPs reached equilibrium, a slow, steady, and controlled release of the drug would be obtained. However, the majority of drugs would overcome some resistance to diffuse across avidin and PEI to the surface of MNPs and finally into aqueous medium. A high concentration of IDAU connected to MNPs might need more proteins and polymers and create conversely more resistance to hold back the effective drug release. Therefore, a low concentration of released IDAU present in the aqueous medium would be obtained.

3.3.2. Toxicity in Cell Culture. The potential of AMNPs to be used as a carrier for IDAU was evaluated in vitro by comparing the cytotoxicity of four formulations: free

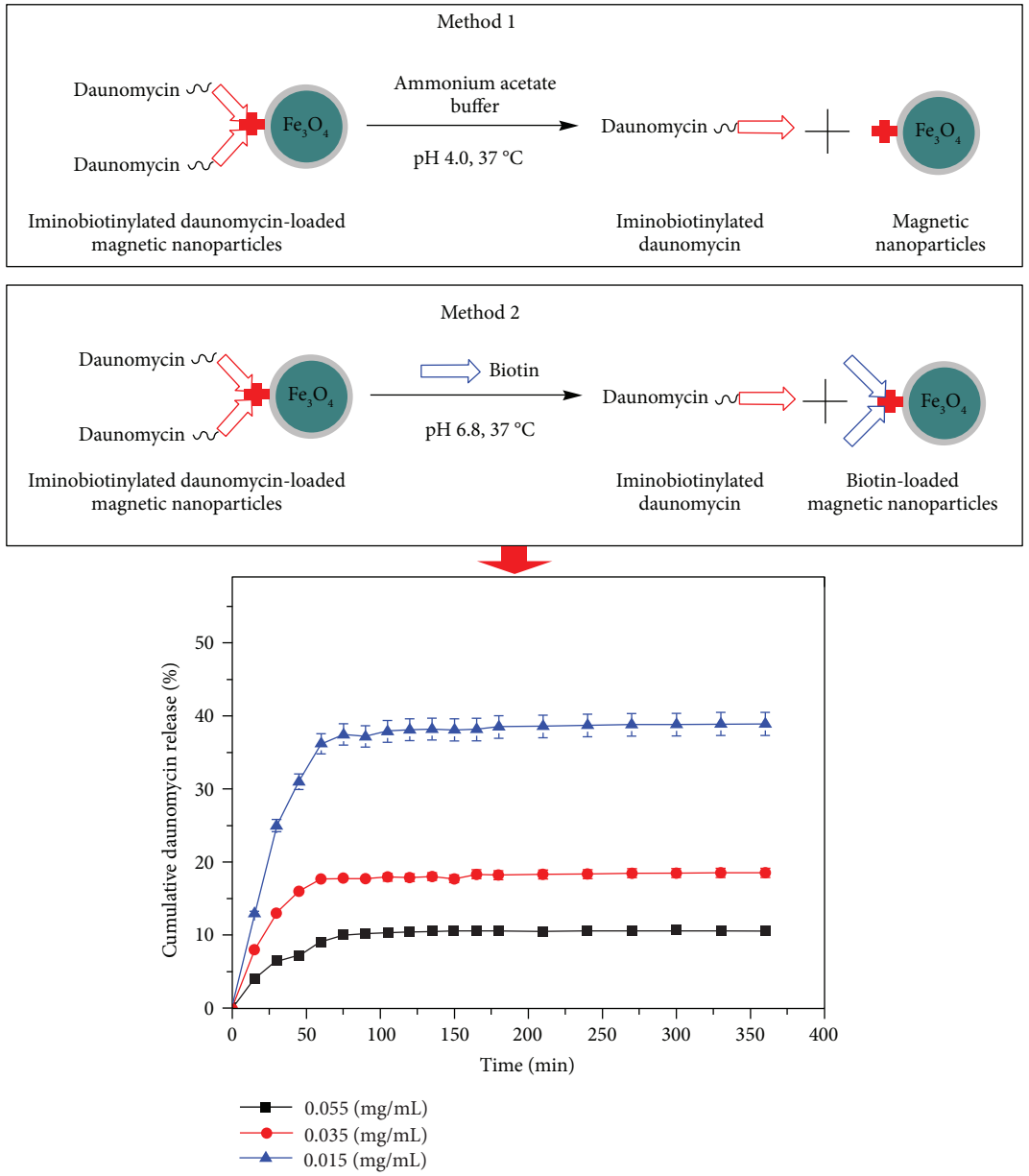

Figure 7: Two methods for releasing of iminobiotinylated daunomycin from nanoparticles and drug release behavior as a function of loaded iminobiotinylated daunomycin concentration (0.015 mg/mL (blue triangle), 0.035 mg/mL (red circle), and 0.055 mg/mL (black square)). Each result is the average calculated in 95% confidence interval of five parallel studies.

DAU (Sample 1), 0.04 mg/mL; IDAU (sample 2), 0.06 mg/mL; IDAU-MNPs (the concentration of IDAU on the surface was 0.06 mg/mL, sample 3); and unloaded MNPs (AMNPs, sample 4), 0.15 mg/mL. The in vitro models chosen for investigating the potential of these materials were the DLKP cell line, and 50% inhibitory concentrations (IC50) of the four samples were determined. As depicted in Figure 8, the results indicated that the IC50 of IDAU was $(1.60 \pm 0.05) \times 10^{-3}$ mg/mL, and it retained significant activity against DLKP cells ($P < 0.05$), although its antitumor activity was lower than that of free DAU. The IC50 of IDAU-MNPs was 0.02 ± 0.007 mg/mL and was much lower than that of free DAU or IDAU, but the presence of low activity against DLKP cells confirmed that a small quantity of IDAU on the surface of MNPs stretched in aqueous medium and interacted with tumor cells. Another reason that IDAU-MNPs had anticancer activity in vitro was a pumping mechanism that enabled diffusion of the drug out of avidin on the surface of nanoparticles [46–48].

The above experimental data clearly demonstrated that IDAU could not only be adsorbed, transported, and released controllably on the surface of MNPs but also exhibited high inhibitory activity against DLKP cells. However, since the delivery of the drug from MNPs carriers in vivo was a complex process, the effectiveness of the present method needs to be further verified. Furthermore, the in vivo tumor inhibition experiments in the external magnetic field are in progress in our research group, and IDAU-MNPs are supposed

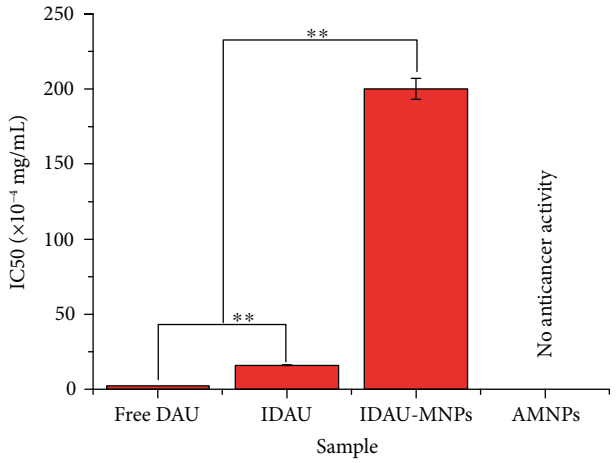

Figure 8: Fifty percent inhibitory concentrations (IC50) of free DAU (sample 1), IDAU (sample 2), IDAU-MNPs (sample 3), and unloaded MNPs (AMNPs, sample 4). Each result is the average calculated in 95% confidence interval of five parallel studies $^{**}P < 0.01$.

to achieve the magnetic drug targeting and improve the therapeutic efficacy.

4. Conclusion

We described here a novel experimental approach to the design and preparation of IDAU-MNPs through the affinity interaction between IDAU and AMNPs. DAU was first 2-iminobiotinylated, which was then attached to AMNPs using the avidin-iminobiotin system. The results obtained using RP-HPLC studies indicated that the optimal acylation rate of IDAU was $78.90 \pm 2.13\%$. The results obtained using FTIR studies strongly suggested that IDAU could be firmly affixed to AMNPs using the avidin-iminobiotin system. The study also found that the loading capacity and efficiency of nanoparticles were mainly dependent on affinity interaction between IDAU and AMNPs, which was impacted obviously by the initial concentration of IDAU. Under the conditions of pH 6.8 and 1 mmol/L of biotin, the drug release was characterized by an initial rapid drug release followed by a slow, steady and controlled release of the drug. The effect of IDAU on DLKP proliferation was tested, the results showed that IC50 was $(1.60 \pm 0.05) \times 10^{-3}$ mg/mL. It could come to a conclusion that the drug had good inhibitory effect on tumor cell growth.

Data Availability

The data used to support the findings of this study are available from the corresponding author upon request.

Conflicts of Interest

The authors declare that there are no conflicts of interest regarding the publication of the paper.

Acknowledgments

The work was supported by the Key Technology R&D Program of Hunan Province of China (Grant no. 2016NK2146), key scientific research projects of Tibet Autonomous Region of China (Project code no. ZD20170014), and National Natural Science Foundation of China (Grant nos. 31360367 and 31571911).

References

[1] N. P. E. Barry and P. J. Sadler, "Exploration of the medical periodic table: towards new targets," *Chemical Communications*, vol. 49, no. 45, pp. 5106–5131, 2013.

[2] E. M. Greer, C. V. Cosgriff, and O. Lavinda, "Towards the development of new anticancer drugs: the Bergman cyclization of an 11-membered ring-constrained enediynes," in *Abstracts of Papers of the American Chemical Society*, vol. 244, American Chemical Society, 1155 16th St, NW, Washington, DC 20036 USA, 2012.

[3] X. Jiang, Y. Sun, J. Yao et al., "Core scaffold-inspired concise synthesis of chiral spirooxindole-pyranopyrimidines with broad-spectrum anticancer potency," *Advanced Synthesis & Catalysis*, vol. 354, no. 5, pp. 917–925, 2012.

[4] C. Dufes, M. Al Robaian, and S. Somani, "Transferrin and the transferrin receptor for the targeted delivery of therapeutic agents to the brain and cancer cells," *Therapeutic Delivery*, vol. 4, no. 5, pp. 629–640, 2013.

[5] W. Li, Y. Cai, Q. Zhong, Y. Yang, S. C. Kundu, and J. Yao, "Silk sericin microcapsules with hydroxyapatite shells: protection and modification of organic microcapsules by biomimetic mineralization," *Journal of Materials Chemistry B*, vol. 4, no. 2, pp. 340–347, 2016.

[6] F. Dilnawaz and S. K. Sahoo, "Enhanced accumulation of curcumin and temozolomide loaded magnetic nanoparticles executes profound cytotoxic effect in glioblastoma spheroid model," *European Journal of Pharmaceutics and Biopharmaceutics*, vol. 85, no. 3, pp. 452–462, 2013.

[7] F. Dilnawaz, A. Singh, S. Mewar, U. Sharma, N. R. Jagannathan, and S. K. Sahoo, "The transport of non-surfactant based paclitaxel loaded magnetic nanoparticles across the blood brain barrier in a rat model," *Biomaterials*, vol. 33, no. 10, pp. 2936–2951, 2012.

[8] Q. Zhang, J. Tong, H. Chen et al., "A novel magnetic nanoparticle hyperthermia combined with ACMF-dependant drug release by DAMMs injection in VX-2 liver tumors," *Journal of Nanoscience and Nanotechnology*, vol. 12, no. 1, pp. 127–131, 2012.

[9] K. K. Jain, "Current status and future prospects of drug delivery systems," *Methods in Molecular Biology*, vol. 1141, pp. 1–56, 2014.

[10] D. Shetty, J. K. Khedkar, K. M. Park, and K. Kim, "Can we beat the biotin–avidin pair?: cucurbit[7]uril-based ultrahigh affinity host–guest complexes and their applications," *Chemical Society Reviews*, vol. 44, no. 23, pp. 8747–8761, 2015.

[11] D. Torrecilla, M. V. Lozano, E. Lallana et al., "Anti-tumor efficacy of chitosan-g-poly(ethylene glycol) nanocapsules containing docetaxel: anti-TMEFF-2 functionalized nanocapsules vs. non-functionalized nanocapsules," *European Journal of Pharmaceutics and Biopharmaceutics*, vol. 83, no. 3, pp. 330–337, 2013.

[12] Z. Fan, M. Shelton, A. K. Singh, D. Senapati, S. A. Khan, and P. C. Ray, "Multifunctional plasmonic shell–magnetic core nanoparticles for targeted diagnostics, isolation, and photothermal destruction of tumor cells," *ACS Nano*, vol. 6, no. 2, pp. 1065–1073, 2012.

[13] J. Gautier, E. Munnier, A. Paillard et al., "A pharmaceutical study of doxorubicin-loaded PEGylated nanoparticles for magnetic drug targeting," *International Journal of Pharmaceutics*, vol. 423, no. 1, pp. 16–25, 2012.

[14] M. G. Krukemeyer, V. Krenn, M. Jakobs, and W. Wagner, "Magnetic drug targeting in a rhabdomyosarcoma rat model using magnetite-dextran composite nanoparticle-bound mitoxantrone and 0.6 tesla extracorporeal magnets – sarcoma treatment in progress," *Journal of Drug Targeting*, vol. 20, no. 2, pp. 185–193, 2012.

[15] S. K. Sahu, S. Maiti, A. Pramanik, S. K. Ghosh, and P. Pramanik, "Controlling the thickness of polymeric shell on magnetic nanoparticles loaded with doxorubicin for targeted delivery and MRI contrast agent," *Carbohydrate Polymers*, vol. 87, no. 4, pp. 2593–2604, 2012.

[16] R. Bayford, T. Rademacher, I. Roitt, and S. X. Wang, "Emerging applications of nanotechnology for diagnosis and therapy of disease: a review," *Physiological Measurement*, vol. 38, no. 8, pp. R183–R203, 2017.

[17] M. David-Pur, L. Bareket-Keren, G. Beit-Yaakov, D. Raz-Prag, and Y. Hanein, "All-carbon-nanotube flexible multi-electrode array for neuronal recording and stimulation," *Biomedical Microdevices*, vol. 16, no. 1, pp. 43–53, 2014.

[18] X. L. Liu, E. S. G. Choo, A. S. Ahmed et al., "Magnetic nanoparticle-loaded polymer nanospheres as magnetic hyperthermia agents," *Journal of Materials Chemistry B*, vol. 2, no. 1, pp. 120–128, 2014.

[19] Q. Pankhurst, S. Jones, and J. Dobson, "Applications of magnetic nanoparticles in biomedicine: the story so far," *Journal of Physics D: Applied Physics*, vol. 49, no. 50, article 501002, 2016.

[20] S. Sharma, K. Sethi, and I. Roy, "Magnetic nanoscale metal-organic frameworks for magnetically aided drug delivery and photodynamic therapy," *New Journal of Chemistry*, vol. 41, no. 20, pp. 11860–11866, 2017.

[21] E. Tombácz, R. Turcu, V. Socoliuc, and L. Vékás, "Magnetic iron oxide nanoparticles: recent trends in design and synthesis of magnetoresponsive nanosystems," *Biochemical and Biophysical Research Communications*, vol. 468, no. 3, pp. 442–453, 2015.

[22] P. Sharma, A. Sharma, M. Sharma et al., "Nanomaterial fungicides: in vitro and in vivo antimycotic activity of cobalt and nickel nanoferrites on phytopathogenic fungi," *Global Challenges*, vol. 1, no. 9, article 1700041, 2017.

[23] S. F. Bakshi, N. Guz, A. Zakharchenko et al., "Nanoreactors based on DNAzyme-functionalized magnetic nanoparticles activated by magnetic field," *Nanoscale*, vol. 10, no. 3, pp. 1356–1365, 2018.

[24] R. Orendorff, A. J. Peck, B. Zheng et al., "First in vivo traumatic brain injury imaging via magnetic particle imaging," *Physics in Medicine & Biology*, vol. 62, no. 9, pp. 3501–3509, 2017.

[25] M. Stimac, T. Dolinsek, U. Lampreht, M. Cemazar, and G. Sersa, "Gene electrotransfer of plasmid with tissue specific promoter encoding shRNA against endoglin exerts antitumor efficacy against murine TS/A tumors by vascular targeted effects," *PLoS One*, vol. 10, no. 4, article e0124913, 2015.

[26] E. E. Weinberger, A. Isakovic, S. Scheiblhofer et al., "The influence of antigen targeting to sub-cellular compartments on the anti-allergic potential of a DNA vaccine," *Vaccine*, vol. 31, no. 51, pp. 6113–6121, 2013.

[27] N. Depalo, R. M. Iacobazzi, G. Valente et al., "Sorafenib delivery nanoplatform based on superparamagnetic iron oxide nanoparticles magnetically targets hepatocellular carcinoma," *Nano Research*, vol. 10, no. 7, pp. 2431–2448, 2017.

[28] F. Dilnawaz, S. Acharya, and S. K. Sahoo, "Recent trends of nanomedicinal approaches in clinics," *International Journal of Pharmaceutics*, vol. 538, no. 1-2, pp. 263–278, 2018.

[29] J. R. Heath, "Nanotechnologies for biomedical science and translational medicine," *Proceedings of the National Academy of Sciences of the United States of America*, vol. 112, no. 47, pp. 14436–14443, 2015.

[30] S. Sun, M. Ma, N. Qiu et al., "Affinity adsorption and separation behaviors of avidin on biofunctional magnetic nanoparticles binding to iminobiotin," *Colloids and Surfaces B: Biointerfaces*, vol. 88, no. 1, pp. 246–253, 2011.

[31] Y. Dai, J. DeSano, W. Tang et al., "Natural proteasome inhibitor celastrol suppresses androgen-independent prostate cancer progression by modulating apoptotic proteins and NF-kappaB," *PLoS One*, vol. 5, no. 12, article e14153, 2010.

[32] Y. Meng, W. Tang, Y. Dai et al., "Natural BH3 mimetic (-)-gossypol chemosensitizes human prostate cancer via Bcl-xL inhibition accompanied by increase of Puma and Noxa," *Molecular Cancer Therapeutics*, vol. 7, no. 7, pp. 2192–2202, 2008.

[33] X. Wu, M. Li, Y. Qu et al., "Design and synthesis of novel gefitinib analogues with improved anti-tumor activity," *Bioorganic & Medicinal Chemistry*, vol. 18, no. 11, pp. 3812–3822, 2010.

[34] G. D. Nardo, M. Breitner, S. J. Sadeghi, S. Castrignanò, and G. Gilardi, "FTIR spectroscopy applied to study dynamics and flexibility of human aromatase: SW02.S8–39," *The FEBS Journal*, vol. 280, p. 163, 2013.

[35] S. A. Tatulian, "Structural characterization of membrane proteins and peptides by FTIR and ATR-FTIR spectroscopy," *Methods in Molecular Biology*, vol. 974, pp. 177–218, 2013.

[36] P. Ghosh, G. P. Devi, R. Priya et al., "Spectroscopic and in silico evaluation of interaction of DNA with six anthraquinone derivatives," *Applied Biochemistry and Biotechnology*, vol. 170, no. 5, pp. 1127–1137, 2013.

[37] V. Staneva, G. Ivanova, and M. Simeonova, "Surface modified poly (butyl cyanoacrylate) nanoparticles loaded with indomethacin: preparation and physicochemical characterization," *Bulgarian Chemical Communications*, vol. 47, pp. 93–99, 2015.

[38] O. V. Zemtsova and K. N. Zheleznov, "Synthesis and specific features of mesomorphic behavior of new polysubstituted triphenylenes," *Russian Chemical Bulletin*, vol. 53, no. 8, pp. 1743–1748, 2004.

[39] L. Bai, Y. Chai, R. Yuan, Y. Yuan, S. Xie, and L. Jiang, "Amperometric aptasensor for thrombin detection using enzyme-mediated direct electrochemistry and DNA-based signal amplification strategy," *Biosensors and Bioelectronics*, vol. 50, pp. 325–330, 2013.

[40] C. Liu, S. Wang, C. Fu, H. Li, S. Xu, and W. Xu, "Preparation of surface-enhanced Raman scattering(SERS)-active optical fiber sensor by laser-induced ag deposition and its application in

bioidentification of biotin/avidin," *Chemical Research in Chinese Universities*, vol. 31, no. 1, pp. 25–30, 2015.

[41] Y. Liu, L. Feng, T. Liu et al., "Multifunctional pH-sensitive polymeric nanoparticles for theranostics evaluated experimentally in cancer," *Nanoscale*, vol. 6, no. 6, pp. 3231–3242, 2014.

[42] J. Zhang, J. Li, Y. Ju, Y. Fu, T. Gong, and Z. Zhang, "Mechanism of enhanced oral absorption of morin by phospholipid complex based self-nanoemulsifying drug delivery system," *Molecular Pharmaceutics*, vol. 12, no. 2, pp. 504–513, 2015.

[43] H. R. Jia, H. Y. Wang, Z. W. Yu, Z. Chen, and F. G. Wu, "Long-time plasma membrane imaging based on a two-step synergistic cell surface modification strategy," *Bioconjugate Chemistry*, vol. 27, no. 3, pp. 782–789, 2016.

[44] S. L. Kuan, D. Y. W. Ng, Y. Wu et al., "pH responsive Janus-like supramolecular fusion proteins for functional protein delivery," *Journal of the American Chemical Society*, vol. 135, no. 46, pp. 17254–17257, 2013.

[45] H. Y. Wang, X. W. Hua, H. R. Jia et al., "Enhanced cell membrane enrichment and subsequent cellular internalization of quantum dots via cell surface engineering: illuminating plasma membranes with quantum dots," *Journal of Materials Chemistry B*, vol. 4, no. 5, pp. 834–843, 2016.

[46] K. S. Bielawski and N. J. Sniadecki, "A magnetic post approach for measuring the viscoelasticity of biomaterials," *Journal of Microelectromechanical Systems*, vol. 25, no. 1, pp. 153–159, 2016.

[47] M. C. Chen, H. A. Chan, M. H. Ling, and L. C. Su, "Implantable polymeric microneedles with phototriggerable properties as a patient-controlled transdermal analgesia system," *Journal of Materials Chemistry B*, vol. 5, no. 3, pp. 496–503, 2017.

[48] C. G. Madsen, A. Skov, S. Baldursdottir, T. Rades, L. Jorgensen, and N. J. Medlicott, "Simple measurements for prediction of drug release from polymer matrices-solubility parameters and intrinsic viscosity," *European Journal of Pharmaceutics and Biopharmaceutics*, vol. 92, pp. 1–7, 2015.